Sensors and Actuators B 237 (2016) 350–357

Contents lists available at ScienceDirect

Sensors and Actuators B: Chemical

journal homepage: www.elsevier.com/locate/snb

Self-assembly gridding α-MoO_3 nanobelts for highly toxic H_2S gas sensors

Lei Zhang[a,1], Zhongli Liu[b,1], Long Jin[a], Binbin Zhang[a], Haitao Zhang[a], Minhao Zhu[a], Weiqing Yang[a,c,*]

[a] Key Laboratory of Advanced Technologies of Materials (Ministry of Education), School of Materials Science and Engineering, Southwest Jiaotong University, Chengdu 610031, China
[b] College of Physics and Electronic Information, Luoyang Normal University, Luoyang 471022, China
[c] State Key Laboratory of Electronic Thin films and Integrated Devices, University of Electronic Science and Technology of China, Chengdu 610054, China

ARTICLE INFO

Article history:
Received 30 March 2016
Received in revised form 7 June 2016
Accepted 18 June 2016
Available online 18 June 2016

Keywords:
H_2S gas sensor
MoO_3
Ab initio molecular dynamics
Electronic local functions

ABSTRACT

We reported the highly toxic H_2S sensor based on self-assembly gridding α-MoO_3 nanobelts prepared by electron beam vapor deposition method. With three dimensional surface modification of porous structures that self-assembly gridding α-MoO_3 nanobelts constructed, this sensor could detect H_2S gas with the concentration of as low as 1 ppm and also possess the excellent selectivity and stability. More importantly, the ab initio molecular dynamics simulations was employed to elucidate the H_2S gas adsorption mechanisms of sensor based on MoO_3 nanobelts by calculating three-dimensional dynamically changing images of electronic local functions of H_2S-MoO_3 interface, firstly and directly predicting the interfacing action between H_2S and MoO_3. It unambiguously suggests the capability of self-assembly gridding α-MoO_3 nanobelts acting as a high toxic H_2S gas sensor for environmental monitoring and safety forecast of poisonous gas in agricultural, industrial and medical fields, and the scientific significance in sight into the gas mechanisms of gas sensors alike.

1. Introduction

As is generally known, a certain amount of H_2S will be badly dangerous to human body or even threat to life. American Conference of Government Industrial Hygienists (ACGIH) has established H_2S gas safety standards with the threshold limit value of 10 ppm [1–3]. When the concentration of H_2S is higher than 250 ppm, it may bring about death. Therefore, it is of great interest to develop a reliable and effective H_2S gas sensor.

Recently, many groups have reported H_2S gas sensors which were prepared by using different nanomaterials from various methods. Firstly, the vertically aligned CuO nanowire array sensors could detect H_2S with the concentration of 500 ppb–1000 ppm [4]. Furthermore, the novel nanosensors based on hybrid polyaniline (PANI) [5] and single-walled carbon nanotubes (SWCN) [6] with gold nanoparticles could sense H_2S in air at room temperature. However, the response and recovery times of the above-mentioned H_2S gas sensors were as long as 2 min–8 min, suggesting it difficult to push forward the practical applications. To achieve this, some H_2S gas sensors based on ZnO nanorods [7,8], NiO porous nanowall arrays [9,10], different CuO nanostructures [11–16], In_2O_3 nanoparticles [17], metals ions doping WO_3 and MoO_3 nanowires [18–24] were designed to improve the response/recovery times for detecting highly toxic H_2S gas. However, there are still many challenges toward the widely commercial applications, such as the bad selectivity and stability. More importantly, due to no systemically theoretical investigations, the adsorption process and interfacing interaction between H_2S gas and sensor materials have been greatly ambiguous to date. Here, we reported a novel highly toxic H_2S sensor based on self-assembly gridding α-MoO_3 nanobelts prepared by electron beam vapor deposition method. The MoO_3 nanobelts has been interdigitally stacked to orderly form three dimensional porous structures. With three dimensional surface modification of these porous structures, this sensor can detect H_2S gas with the concentration of as low as 1 ppm, possess the excellent selectivity in comparison with CO, methanol, NH_3, Ethanol and totriethylamine (TEA), and render the robustness of 92% after 3000 response/recovery cycles. More importantly, the ab initio molecular dynamics (AIMD) simulations

* Corresponding author at: Key Laboratory of Advanced Technologies of Materials (Ministry of Education), School of Materials Science and Engineering, Southwest Jiaotong University, Chengdu 610031, China.
E-mail address: wqyang@swjtu.edu.cn (W. Yang).
[1] These authors contributed equally to this work.

http://dx.doi.org/10.1016/j.snb.2016.06.104
0925-4005/

was employed to elucidate the H_2S gas adsorption mechanisms of sensor based on MoO_3 nanobelts. The 3-dimensional dynamically changing images of electronic local functions (ELF) of H_2S-MoO_3 interfacing were firstly simulated to predict the interfacing action between H_2S and MoO_3. Therefore, it evidently suggests the self-assembly gridding α-MoO_3 nanobelts could be employed to prepare a highly toxic H_2S gas sensor for environmental monitoring and safety forecast of poisonous gas in agricultural, industrial and medical fields, and AIMD simulations should be a potential method to reveal the gas mechanisms of gas sensors alike.

2. Experimental and Theoretical

2.1. Preparation of self-assembly gridding α-MoO_3 nanobelts

MoO_3 nanobelts were deposited by electron beam evaporation with the evaporation material MoO_3 pellets (purity 99.99%). The MoO_3 powder was ball milled for 2 h by using the high energy ball mill, then dried at a 473 K for 2 h and then made into pellets with diameter of 15 mm. The MoO_3 targets were sintered at 673 K for 1 h in air. Firstly, the vacuum chamber was initially pumped down to a pressure of 1×10^{-4} Pa before evaporation and the working pressure was being controlled at about 1×10^{-3} Pa throughout the evaporating process. The quartz substrate temperatures were maintained at 300 °C and the distance between the target and the substrate was about 4 cm. Subsequently, after the substrate temperature had been steady-going at the set temperature for 10 min, the MoO_3 pellet was heated using an electron beam which was collimated from the direct current heated cathode of tungsten filament. The surface of MoO_3 pellet was scanned using a 270° deflected electron beam at an accelerating voltage of 6 kV. The material evaporated from the MoO_3 target had been deposited on the quartz substrates for 5 min. Finally, the samples were carefully taken out after the substrate temperature gradually came down to the room temperature.

2.2. Fabrication and gas measurement of gas sensor

For gas sensing measurements, gas sensor device was constructed. Firstly, the copper thin film as gas sensor electrode was deposited on MoO_3 nanobelts/quartz substrates by direct current magnetic sputtering method. Then, as-grown gas sensors was put in the tube furnace. Finally, gas sensors were measured by SMU (Agilent B2901A) in sealed chamber at the working temperature ranging from 300 K to 600 K and under the humidity of 20%.

2.3. Theoretical simulations details

The AIMD simulations were performed with the CP2 K molecular simulation software suite [25]. All the simulations were performed in the canonical (NVT) ensemble at 450 K and zero pressure. The supercell contained 7 MoO_3 layers and 15 H_2S molecules with 24 Å vacuum. The motions of ions and electrons in the AIMD simulations were realized by the Born-Oppenheimer approximation. The interatomic potentials were calculated on the fly by directly solving the Schrödinger equation. A 300 Ry cutoff was tested to sufficiently converge the total energy to 10^{-8} Ry. The simulation supercell contained 493 atoms in total (112 MoO_3 and 15H_2S). The Γ point in the reciprocal space is tested to be sufficient to converge the pressure and temperature well [26]. The optimized double zeta valence polarized basis set [27] was used for all atoms. We applied the local-density approximations (LDA) exchange-correlation functional parametrized by Goedecker, Teter and Hutter (GTH) [28]. We have tested the GGA functional and found that the process of adsorption was much slower, and it yielded the similar end adsorption characteristics as the LDA. While, the LDA is much cheaper than the GGA with the cp2k code, and thus we mainly adopted the LDA to qualitatively described the dynamic adsorption process. The pseudopotentials of Mo, O, S, and H atoms were generated with valence configurations $4d^5 5s^1$, $2s^2 2p^4$, $3s^2 3p^4$, and $1s^1$, respectively. The time step of 1 fs and total run time of 5 ps were used to equilibrate the system adequately in our AIMD simulations. As shown in Fig. S5, using much shorter run time (2.5 ps) we can also simulate the adsorption process qualitatively. The wavefunction convergence criterion of 10^{-4} Ry can converge pressure and temperature well.

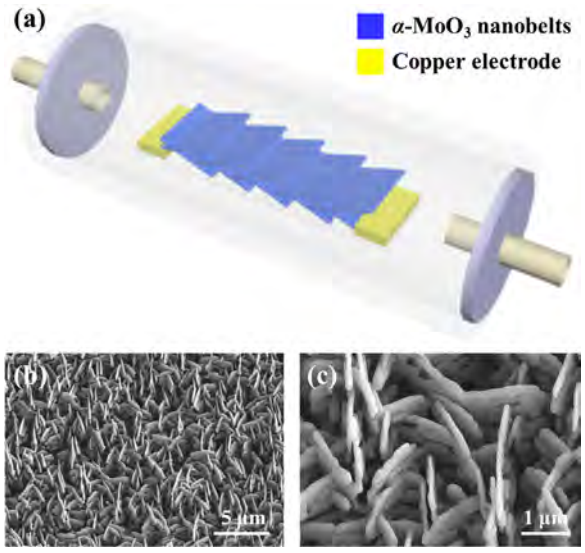

Fig. 1. (a) The sketch of H_2S gas sensor setup, (b) SEM image and (c) enlarged SEM image of self-assembly gridding α-MoO_3 nanobelts.

3. Results and discussions

3.1. Morphology characterization and crystal structure

Fig. 1 presents the diagram of gas-testing setup and morphology characterization of gridding α-MoO_3 nanobelts. Fig. 1a shows a sketch of gas-testing setup, in which, the heater, commercial temperature sensor and gridding α-MoO_3 nanobelts gas sensor were integrated in chamber. The copper thin films as an electrode were deposited by DC magnetron sputtering techniques. Fig. 1b and 1c present the SEM image and its enlarged view of α-MoO_3 nanobelts, in which, α-MoO_3 nanobelts were orderly stacked and self-assembly grown on the quartz substrates. The relatively well-distributed α-MoO_3 nanobelts with the thickness of about 100 nm and the length of about 2 μm were regularly interconnected to form the stable three-way supports. These supports were orderly stacked to construct 3D porous gridding honeycomb, which is in favor of the fine performance of gas sensor due to the remarkably increasing contact area between H_2S gas and α-MoO_3 nanobelts. Additionally, this kind of unique 3D porous gridding honeycomb structure and the longer MoO_3 nanobelts can dramatically decrease the connection point numbers to cut down the contact resistance (R_c) and effectively to lower down the total resistance of sensors ($R = R_c + R_b$, R_b is the bulk resistance of materials). [29–31] The detailed derivation of R was presented in Fig. S1. To our knowledge, such an interesting structure as self-assembly gridding MoO_3 nanobelts has been never reported to date.

Fig. 2a suggests that MoO_3 should be a typical α-MoO_3 phase due to its characteristic peaks (0k0) (k = 2, 4 and 6), which can be indexed with the orthorhombic structure with the lattice constants of a = 3.962 Å, b = 13.858 Å, c = 3.697 Å and Pbnm (62) space group (PDF# 05-0508) [32–35]. Moreover, the α-MoO_3 nanobelts

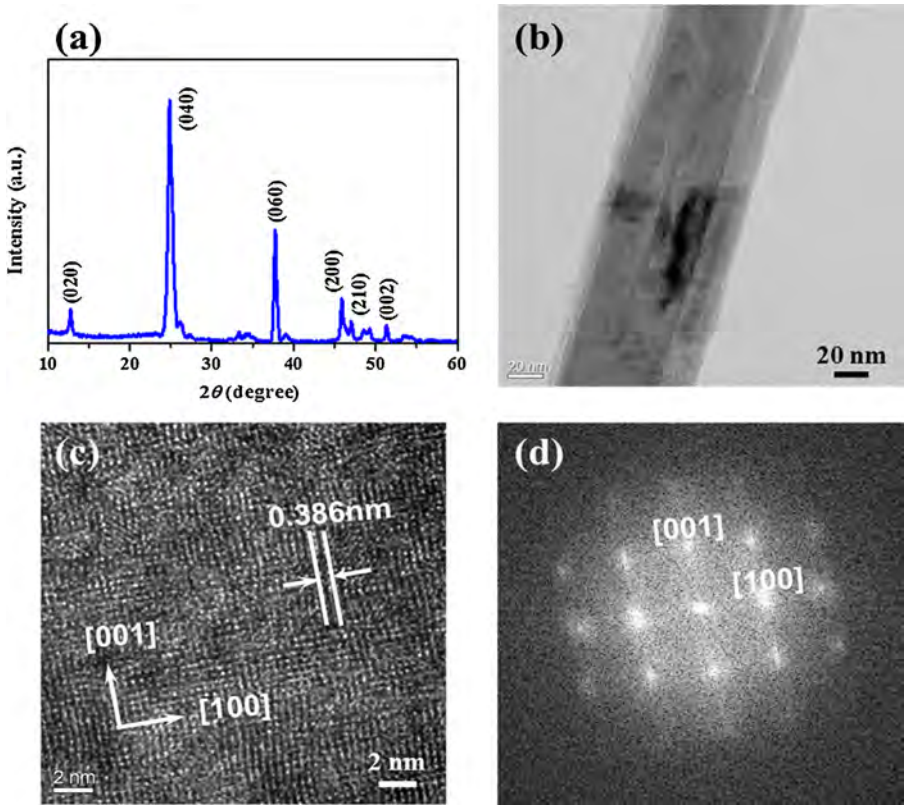

Fig. 2. The crystal characterization of self-assembly gridding α-MoO_3 nanobelts. (a) XRD pattern. (b) TEM image. (c) HRTEM image. (d) The image of selected-area electron diffraction pattern.

had a preferred orientation with the *b*-axis normal to the quartz substrates. Besides, the nanobelts-like α-MoO_3 was further characterized and confirmed by transmission electron microscopy (TEM) technique (Fig. 2b) and the high-resolution transmission electron microscopy (HRTEM) image (Fig. 2c). The selected-area electron diffraction (SAED) (Fig. 2d) pattern was recorded with the incident electron beam perpendicular to [010] of α-MoO_3 nanobelts, indicating its growth direction, top/bottom surfaces and side surfaces should be [001], [010] and [100], respectively.

3.2. Gas sensing properties of α-MoO_3 sensors

The responses of α-MoO_3 sensors to highly toxic H_2S gas with different concentrations were measured at the different operating temperatures of 300 K–600 K. Fig. 3 demonstrates the applications of self-assembly gridding α-MoO_3 nanobelts as highly toxic H_2S gas sensors at the temperature of 300 K, 450 K and 600 K. We measured the H_2S gas detecting performance of α-MoO_3 nanobelts with the gas concentrations from 1 ppm to 100 ppm. The sensitivity *S* is defined as, [29–31,36].

$$S = R_a/R_g \times 100\% \quad (1)$$

where R_a and R_g are the resistance of α-MoO_3 nanobelts sensor in air and in the target gas H_2S mixed with air, respectively. From Fig. 3a1–c1, this gas sensor can effectively detect the toxic H_2S gas with the concentration of as low as 1 ppm. Their sensitivities *S* are shown in Fig. 3a2–c2, obviously revealing that the operating temperature should dramatically affect the toxic H_2S gas detecting performance of α-MoO_3 nanobelts sensor. As we know, at relatively low temperature, the surface of nanobelts preferentially adsorbs O_2^- and its sensitivity is consequently poor due to the lower reactiveness of O_2^-. Furthermore, when the operating temperature increases, the surface of materials mainly adsorbs O^- (or O^{2-}) with the higher reactiveness. However, if the temperature increases too much, lots of oxygen ionic species adsorbed previously will desorb ahead of schedule, resulting in the decreasing sensitivity of materials for target gas [36]. From Fig. 3, the best operating temperature of MoO_3 nanobelts for target gas H_2S should be about 450 K, which is lower than that of other n-type metal-oxides for the same target gas H_2S, such as In_2O_3 nanofibers (533 K) [37] and SnO_2 nanofibers (573 K) [38]. Such low optimal operating temperature may be ascribed to the relatively fewer connection point numbers of the unique 3D porous gridding honeycomb structure. Additionally, the sensitivity of this sensor gradually increases with the concentration of H_2S gas ranging from 1.23 to 223. And the corresponding sensitivity *S* at 450 K is as high as 223 at the concentration of 100 ppm, evidently promising a supersensitive toxic H_2S gas sensor based on the self-assembly gridding α-MoO_3 nanobelts.

Similar to all the other gas sensors, the selectivity and stability are still two great challenges for the practical application of H_2S sensor. Fig. 4a presents the selectivity of H_2S to NH_3, acetone, methanol, CO and TEA with the concentration of 100 ppm at the operating temperatures of 450 K. This result obviously reveals that this sensor not only shows the higher sensitivity to H_2S but also exhibits the better selectivity to NH_3, acetone, methanol, CO and TEA. Though all these target gases are the reducing gas, the optimal operating temperature (450 K) of H_2S should be quite different from that of other five reducing gases. Additionally, it may be attributed to different reaction dynamics of other gases and H_2S with adsorbed oxygen species on the surfaces of the sensing materials (please see the Supplementary materials). From Fig. 4a, the sensitivity of as-grown samples for TEA is comparatively high for the selectivity properties and we further expanded the working temperature measurement. As shown in Fig. S2, the optimal working temperature for TEA is 550 K and different from the working temperature for H_2S gas (450 K), which is in good agreement with

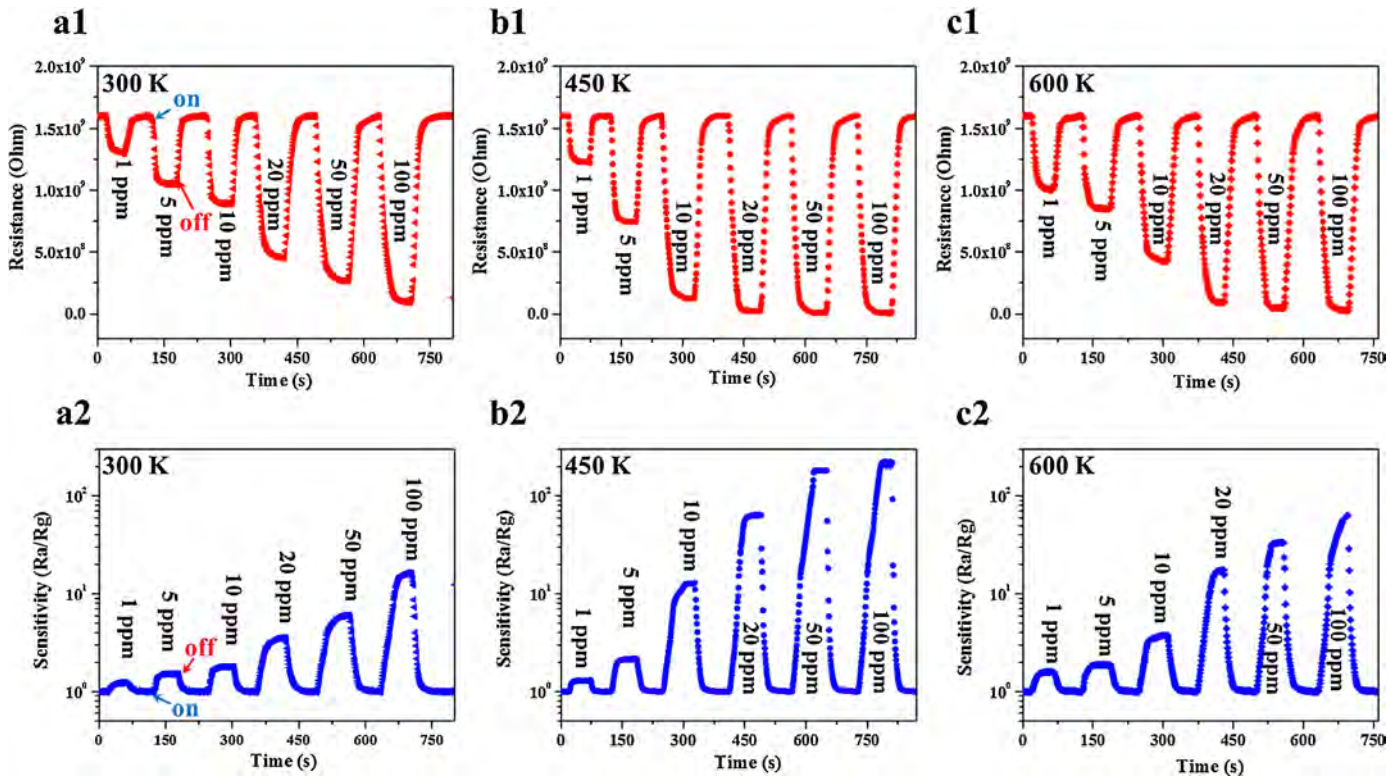

Fig. 3. Temperature depended sensing performance. (a1–c1) The responses of α-MoO_3 sensors to highly toxic H_2S gas with different concentrations were measured at the different operating temperatures of 300 K, 450 K and 600 K. (a2–c2) The sensitivity of α-MoO_3 nanobelts with various H_2S concentrations at the different operating temperature of 300 K, 450 K and 600 K.

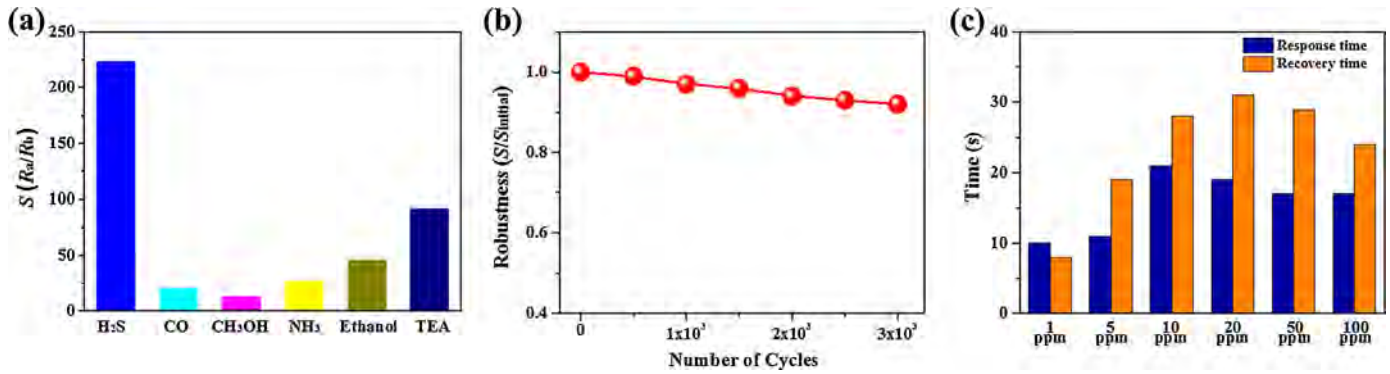

Fig. 4. The study of α-MoO_3 sensors toward selectivity and stability. (a) The sensitivity toward H_2S in comparison to other toxic species (CO, Methanol, NH_3, Ethanol and TEA); (b) Robustness values at the H_2S gas concentration of 100 ppm; (c) the detailed response/recover times to H_2S gas at the operating temperature of 450 K.

the results that Li-Hua Huo group reported [39]. Therefore, the as-grown samples generously presents the good selectivity for H_2S gas. Such a good sensitivity may be ascribed to the reason that molybdenum oxide react with H_2S at the working temperature of 450 K to form the molybdenum sulfide-oxide heteronanostructures. [40,41] As shown in Fig. 4b, the sensitivity of this sensor is still 92% of its initial value after 3000 recycles, evidently presenting its excellent stability. Moreover, from the SEM images of nanobelts after 3000 cycles in Fig. S3, the main structure of 3D porous gridding honeycomb did not change except for a little change of nanobelts surface due to the interfacing interaction of MoO_3 nanobelts and target gas H_2S. Besides, Fig. 4c shows the response and recover time to H_2S gas at the operating temperature of 450 K are controlled within 10–21 s and 8–31 s, respectively. Therefore, these excellent performances of H_2S gas based on self-assembly gridding α-MoO_3 nanobelts unambiguously renders great potential applications for environmental monitoring and safety forecast of poisonous gas in agricultural, industrial and medical fields.

3.3. *Sensing mechanism of α-MoO_3 sensors*

Fig. S4 sketches the sensing mechanism of sensors. When the sensor is exposed to air, oxygen molecules can adsorb on the surface of MoO_3 nanobelts and form chemisorbed oxygen species (O^{-2}, O^- and O^{2-}) by capturing electrons from the adsorption sites on the oxide surface, resulting in the thicker surface depletion region. [29–31,36]. Once the sensor is exposed to the toxic H_2S gas, this gas may interact with the pre-absorbed oxygen species and release a few trapped electrons back to the conduction band, which results in the rapid decrease of surface depletion region and the quick increase of conductance region. This will eventually lead

to a decrease in the surface resistance of self-assembly gridding α-MoO_3 nanobelts.

In order to further understand the dynamic absorption process of H_2S on the (0001) surface of α-MoO_3, we conducted systematic AIMD simulations, equivalent to the experimental environment. In detail, we first fully relaxed the positions of all the atoms in the unit cell with 16 atoms. Then, we built the supercell by expanding the unit cell with the multiplications of $2 \times 2 \times 7$. The 15 H_2S molecules were then placed on the (0001) surface of α-MoO_3 supercell with the distance of 3 Å. It was verified that the initial positions of the H_2S molecules do not affect the simulation results. The relaxation of atoms and chemical reactions was performed in the canonical (NVT) ensemble at 450 K. The pressure of system fluctuated around 0 GPa.

The electronic localization functions (ELF) is a measure for the likelihood of finding an electron in the neighborhood space of a reference electron located at a given point and with the same spin. The ELF is defined by $ELF(\boldsymbol{r}) = 1/[1 + \chi(\boldsymbol{r})]$, where $\chi(\boldsymbol{r})$ is the function of electron density and a dimensionless localization index that expresses electron localization with respect to the uniform electron gas. The value of ELF is then located in the range of [0, 1]. ELF = 1 corresponds to perfect localization and ELF = 0.5 corresponds to the uniform electron gas. The ELF of the whole H_2S-MoO_3 system were also carefully calculated and analyzed. The slices of the ELF H_2S-MoO_3 interface can help to discover the evolution process of electronic surface states.

The snapshots at different absorption stages in the whole dynamic process are illustrated in Fig. 5. As shown in Fig. 5a1, the first stage of H_2S interaction with MoO_3 is the absorption of H_2S on its (0001) surface, highlighted by the reaction of the H^{atom} with the O^{2-} ion. The physical absorption between H atom and O^{2-} starts shortly according to the nonbonding ELF image as shown in Fig. 5a4. Then, in the second stage the H—O bonds form and are stabilized with time, just as shown in Fig. 5b3 and b4. Fig. 5c1 and d1 imply that H_2S dissociation ratio increases and the number of H—O bonds grows with simulation time. In the final stage, the bonding formation of H atom and O^{2-} extend to the internal O^{2-} layer adjacent to the outmost one as illustrated in Figs. 5c1–f1. It is also observed that, wherever the bonding of H—O occurs, it is strengthened and stabilized when the system goes to equilibration, as is reflected in the illustration of Fig. 5d3,d4,e3,e4,f3, and f4. This can be evidenced from the time evolution of the H—O bond length as shown in Fig. S5. This indicates the high activity of O^{2-} ions in the MoO_3 with respective to H atoms from the H_2S molecules. The H_2S molecules mainly dissociate to H and HS, but further dissociation of HS is much difficult, as we did not observe the isolated S atom in the whole simulation process by analyzing the ELF image around S element. The average H—O bond length is 1.07 Å, implying the chemical adsorption nature. For the more elaborate adsorption process, please see Movies S1.

It is also interesting that the (0001) surface reconstructed considerably after the dissociation and reaction of H_2S on α-MoO_3 (Fig. 6). From the comparison of the α-MoO3 (0001) surface structures before (Fig. 6a and b) and after (Fig. 6c and d) the reaction of H_2S with α-MoO3, we note very large dislocations of O^{2-} ions shown in the dashed blue circles in Fig. 6c and d. The (0001) surface becomes obviously rugged after the reaction of H_2S on it (Fig. 6c and d). Furthermore, such reconstructions of atomic dislocations not only take place on the outmost layer, but also on the adjacent inner layers. Just as we have seen from the comparison of the α-MoO3 inner layer structure before (Fig. 6e and f) and after (Fig. 6g and h) structural reconstruction. More importantly, as shown in Fig. 6e–h, these dislocations on the surface layers also bring about voids in the MoO_3. The mobility of O^{2-} ions are much higher than that of Mo^{6+} ions, as is the main driven force of the surface reconstruction and the formation of voids. The reconstruction of the α-MoO_3 (0001) surface observed in the AIMD simulations well explains our experimental SEM observations (Fig.S2) that nanobelts surfaces change slightly resulting from the interfacing interaction of α-MoO_3 nanobelts and target gas H_2S. This reasonable explanation evidently demonstrates the AIMD simulation is a potentially effective method to investigate the gas mechanism of gas sensor alike.

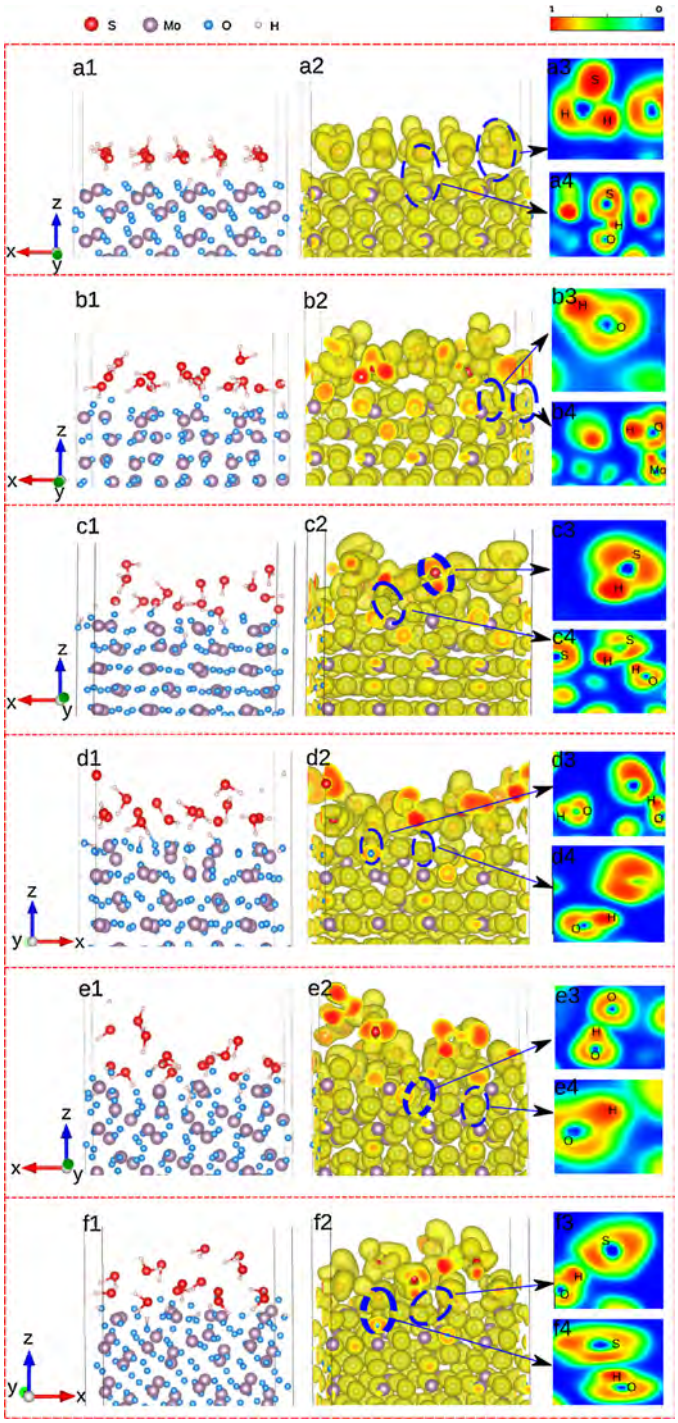

Fig. 5. The dynamic absorption and dissociation evolution process of H_2S on the (0001) surface of MoO_3 from ab initio molecular dynamics simulations at 450 K and zero pressure, along with the electronic local functions (ELF). The slices of the ELF of H—O bonds are also shown.

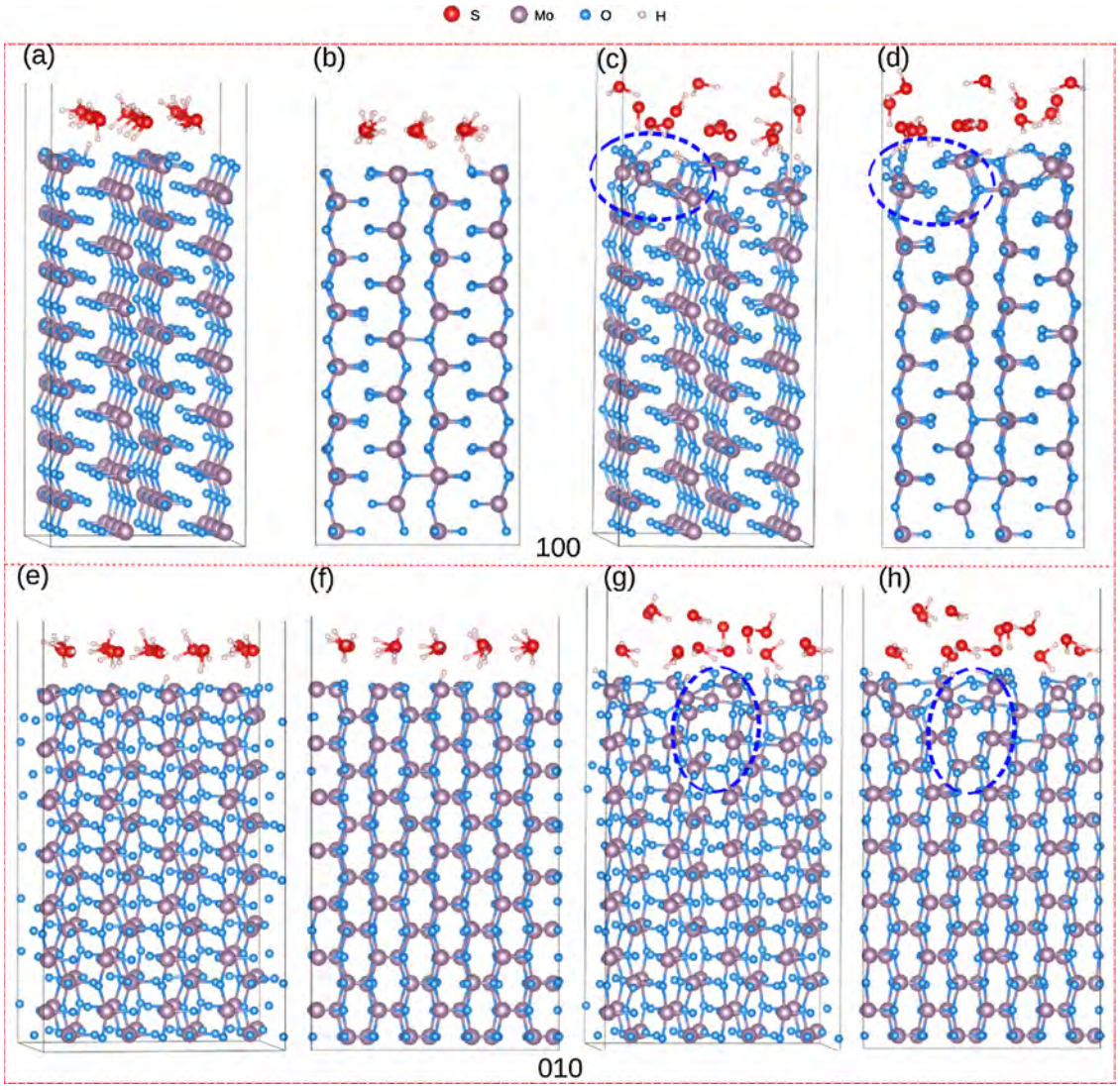

Fig. 6. The structures comparison of α-MoO_3 (0001) surface before and after H_2S absorption. The top panel: the comparison of the α-MoO_3 (0001) surface structures before [(a) and (b)] and after [(c) and (d)] structural reconstruction viewed along the [100] direction. The bottom panel: the comparison of the α-MoO_3 adjacent inner layer structures before [(e) and (f)] and after [(g) and (h)] structural reconstruction viewed along the [010] direction.

4. Conclusions

In summary, we successfully presented a novel highly toxic H_2S sensor based on self-assembly gridding α-MoO_3 nanobelts prepared by electron beam vapor deposition method. This sensor could detect H_2S gas with the concentration of as low as 1 ppm and also possessed the excellent selectivity and stability due to three dimensional surface modification of porous structures that the gridding α-MoO_3 nanobelts constructed. More importantly, by calculating three-dimensional dynamic changing images of electronic local functions (ELF) of H_2S-MoO_3 interface, the AIMD simulations was employed to elucidate the H_2S gas adsorption mechanisms of sensor based on MoO_3 nanobelts, firstly and directly predicting the interfacing reaction between H_2S and MoO_3. The reported work provides an innovative approach to effectively broaden the scope of toxic gas sensors and extend the framework for its potential applications in environmental monitoring and safety forecast of poisonous gas in agricultural, industrial and medical fields.

Competing financial interests

The authors declare no competing financial interests.

Acknowledgements

This work is supported by the National Natural Science Foundation of China (Nos. 51202023 and 11104127), Sichuan Province Science and Technology Plan Project (No. 2015JQ0013) and the Fundamental Research Funds for the Central Universities (A0920502051408-10).

Appendix A. Supplementary data

Supplementary data associated with this article can be found, in the online version, at http://dx.doi.org/10.1016/j.snb.2016.06.104.

References

[1] Y. Wang, S.R. Wang, Y.Q. Zhao, B.L. Zhu, F.H. Kong, D. Wang, et al., H_2S sensing characteristics of Pt-doped alpha-Fe_2O_3 thick film sensors, Sens. Actuators B Chem. 125 (2007) 79–84.
[2] Q.Y. Ouyang, L. Li, Q.S. Wang, Y. Zhang, T.S. Wang, F.N. Meng, et al., Facile synthesis and enhanced H_2S sensing performances of Fe-doped alpha-MoO_3 micro-structures, Sens. Actuators B Chem. 169 (2012) 17–25.
[3] L.Q. Mai, L. Xu, Q.A. Gao, C.H. Han, B. Hu, Y.Q. Pi, Single beta-$AgVO_3$ nanowire H_2S sensor, Nano Lett. 10 (2010) 2604–2608.

[4] J.J. Chen, K. Wang, L. Hartman, W.L. Zhou, H_2S detection by vertically aligned CuO nanowire array sensors, J. Phys. Chem. C 112 (2008) 16017–16021.
[5] M.D. Shirsat, M.A. Bangar, M.A. Deshusses, N.V. Myung, A. Mulchandani, Polyaniline nanowires-gold nanoparticles hybrid network based chemiresistive hydrogen sulfide sensor, Appl. Phys. Lett. 94 (2009) 083502–083502-3.
[6] S. Mubeen, T. Zhang, N. Chartuprayoon, Y. Rheem, A. Mulchandani, N.V. Myung, et al., Sensitive detection of H_2S using gold nanoparticle decorated single-walled carbon nanotubes, Anal. Chem. 82 (2010) 250–257.
[7] L. Liao, H.B. Lu, J.C. Li, H. He, D.F. Wang, D.J. Fu, et al., Size dependence of gas sensitivity of ZnO nanorods, J. Phys. Chem. C 111 (2007) 1900–1903.
[8] Z.S. Hosseini, A.I. Zad, A. Mortezaali, Room temperature H_2S gas sensor based on rather aligned ZnO nanorods with flower-like structures, Sens. Actuators B Chem. 207 (2015) 865–871.
[9] T.T. Yu, X.L. Cheng, X.F. Zhang, L.L. Sui, Y.M. Xu, S. Gao, et al., Highly sensitive H_2S detection sensors at low temperature based on hierarchically structured NiO porous nanowall arrays, J. Mater. Chem. A 3 (2015), 11991–11199.
[10] T.T. Yu, X.F. Zhang, Y.M. Xu, X.L. Cheng, S. Gao, H. Zhao, et al., Low concentration H_2S detection of CdO-decorated hierarchically mesoporous NiO nanofilm with wrinkle structure, Sens. Actuators B Chem. 230 (2016) 706–713.
[11] X.H. Kong, Y.D. Li, High sensitivity of CuO modified SnO_2 nanoribbons to H_2S at room temperature, Sens. Actuators B Chem. 105 (2005) 449–453.
[12] G.J. Sun, S.W. Choi, A. Katoch, P. Wu, S.S. Kim, Bi-functional mechanism of H_2S detection using CuO-SnO_2 nanowires, J. Mater. Chem. C 1 (2013) 5454–5462.
[13] K.I. Choi, H.J. Kim, Y.C. Kang, J.H. Lee, Ultraselective and ultrasensitive detection of H_2S in highly humid atmosphere using CuO-loaded SnO_2 hollow spheres for real-time diagnosis of halitosis, Sens. Actuators B Chem. 194 (2014) 371–376.
[14] Y. Qin, F. Zhang, Y. Chen, Y. Zhou, J. Li, A. Zhu, et al., Hierarchically porous CuO hollow spheres fabricated via a one-pot template-free method for high-performance gas sensors, J. Phys. Chem. C 116 (2012) 11994–12000.
[15] S. Steinhauer, E. Brunet, T. Maier, G.C. Mutinati, A. Kock, O. Freudenberg, et al., Gas sensing properties of novel CuO nanowire devices, Sens. Actuators B Chem. 187 (2013) 50–57.
[16] Y.J. Chen, F.N. Meng, H.L. Yu, C.L. Zhu, T.S. Wang, P. Gao, et al., Sonochemical synthesis and ppb H_2S sensing performances of CuO nanobelts, Sens. Actuators B Chem. 176 (2013) 15–21.
[17] K. Yao, D. Caruntu, Z.M. Zeng, J.J. Chen, C.J. O'Connor, W.L. Zhou, Parts per billion-level H_2S detection at room temperature based on self-assembled In_2O_3 nanoparticles, J. Phys. Chem. C 113 (2009) 14812–14817.
[18] S.L. Bai, C. Chen, D.F. Zhang, R.X. Luo, D.Q. Li, A.F. Chen, et al., Intrinsic characteristic and mechanism in enhancing H_2S sensing of Cd-doped alpha-MoO_3 nanobelts, Sens. Actuators B Chem. 204 (2014) 754–762.
[19] V. Kruefu, A. Wisitsoraat, A. Tuantranont, S. Phanichphant, Ultra-sensitive H_2S sensors based on hydrothermal/impregnation-made Ru-functionalized WO_3 nanorods, Sens. Actuators B Chem. 215 (2015) 630–636.
[20] S.J. Choi, C. Choi, S.J. Kim, H.J. Cho, M. Hakim, S. Jeon, et al., Highly efficient electronic sensitization of non-oxidized graphene flakes on controlled pore-loaded WO_3 nanofibers for selective detection of H_2S molecules, Sci. Rep. 5 (2015) 8067–8076.
[21] S.L. Bai, C. Chen, R.X. Luo, A.F. Chen, D.Q. Li, Synthesis of MoO_3/reduced graphene oxide hybrids and mechanism of enhancing H_2S sensing performances, Sens. Actuators B Chem. 216 (2015) 113–120.
[22] C.S. Rout, M. Hegde, C.N.R. Rao, H_2S sensors based on tungsten oxide nanostructures, Sens. Actuators B Chem. 128 (2008) 488–493.
[23] Y.J. Chen, X.M. Gao, X.P. Di, Q.Y. Ouyang, P. Gao, L.H. Qi, et al., Porous iron molybdate nanorods: in situ diffusion synthesis and low-temperature H_2S gas sensing, ACS Appl. Mater. Interfaces 5 (2013) 3267–3274.
[24] X.M. Gao, C.Y. Li, Z.X. Yin, Y.J. Chen, Synthesis and H_2S sensing performance of $MoO_3/Fe_2(MoO_4)_3$ yolk/shell nanostructures, RSC Adv. 5 (2015) 37703–37709.
[25] J. VandeVondele, M. Krack, F. Mohamed, M. Parrinello, T. Chassaing, J. Hutter, QUICKSTEP: fast and accurate density functional calculations using a mixed Gaussian and plane waves approach, Comput. Phys. Commun. 167 (2005) 103–128.
[26] J. Bouchet, F. Bottin, G. Jomard, G. Zerah, Melting curve of aluminum up to 300 GPa obtained through ab initio molecular dynamics simulations, Phys. Rev. B 80 (2009) 094102–094106.
[27] J. VandeVondele, J. Hutter, Gaussian basis sets for accurate calculations on molecular systems in gas and condensed phases, J. Chem. Phys. 127 (2007) 348–353.
[28] S. Goedecker, M. Teter, J. Hutter, Separable dual-space Gaussian pseudopotentials, Phys. Rev. B 54 (1996) 1703–1710.
[29] M.M. Arafat, B. Dinan, S.A. Akbar, A.S.M.A. Haseeb, Gas sensors based on one dimensional nanostructured metal-oxides: a review, Sensors (Basel) 12 (2012) 7207–7258.
[30] Z. Yang, L.M. Li, Q. Wan, Q.H. Liu, T.H. Wang, High-performance ethanol sensing based on an aligned assembly of ZnO nanorods, Sens. Actuators B Chem. 135 (2008) 57–60.
[31] C.C. Li, Z.F. Du, L.M. Li, H.C. Yu, Q. Wan, T.H. Wang, Surface-depletion controlled gas sensing of ZnO nanorods grown at room temperature, Appl. Phys. Lett. 91 (2007) 032101–032101-3.
[32] W.Q. Yang, Z.R. Wei, M. Gao, Y. Chen, J. Xu, C.L. Chen, et al., Fabrication and field emission properties of needle-shaped MoO_3 nanobelts, J. Alloys Compd. 576 (2013) 332–335.
[33] W.Q. Yang, Z.R. Wei, X.H. Zhu, D.Y. Yang, Strong influence of substrate temperature on the growth of nanocrystalline MoO_3 thin films, Phys. Lett. A 373 (2009) 3965–3968.
[34] N.A. Rae, M.T. Islam, C.T. Chantler, M.D. de Jonge, Energy determination of synchrotron X-ray beam energy in the high energy region of 38–50 keV using powder diffraction patterns of the standard powder Si640b, Nucl. Instrum. Methods A 619 (2010) 147–149.
[35] X.N. Wen, W.Q. Yang, Y. Ding, S.M. Niu, Z.L. Wang, Piezoresistive effect in MoO_3 nanobelts and its application in strain-enhanced oxygen sensors, Nano Res. 7 (2014) 180–189.
[36] B. Karunagaran, P. Uthirakumar, S.J. Chung, S. Velumani, E.K. Suh, TiO_2 thin film gas sensor for monitoring ammonia, Mater. Charact. 58 (2007) 680–684.
[37] W. Zheng, X.F. Lu, W. Wang, Z.Y. Li, H.N. Zhang, Z.J. Wang, et al., Assembly of Pt nanoparticles on electrospun In_2O_3 nanofibers for H_2S detection, J. Colloid Interf. Sci. 338 (2009) 366–370.
[38] K.Y. Dong, J.K. Choi, I.S. Hwang, J.W. Lee, B.H. Kang, D.J. Ham, et al., Enhanced H_2S sensing characteristics of Pt doped SnO_2 nanofibers sensors with micro heater, Sens. Actuators B Chem. 157 (2011) 154–161.
[39] L.L. Sui, Y.M. Xu, X.F. Zhang, X.L. Cheng, S. Gao, H. Zhao, et al., Construction of three-dimensional flower-like alpha-MoO_3 with hierarchical structure for highly selective triethylamine sensor, Sens. Actuators B Chem. 208 (2015) 406–414.
[40] D.Y. Fu, C.L. Zhu, X.T. Zhang, C.Y. Li, Y.J. Chen, Two-dimensional net-like SnO_2/ZnO heteronanostructures for high-performance H_2S gas sensor, J. Mater. Chem. A 4 (2016) 1390–1398.
[41] T.S. Wang, Q.S. Wang, C.L. Zhu, Q.Y. Ouyang, L.H. Qi, C.Y. Li, et al., Synthesis and enhanced H_2S gas sensing properties of alpha-MoO_3/CuO p-n junction nanocomposite, Sens. Actuators B Chem. 171 (2012) 256–262.

Biographies

Lei Zhang is a Ph.D. student in Materials Science and Engineering and began his master's and doctoral studies in 2014. Prior to arriving at Southwest Jiaotong University, Lei completed M.S. degrees at Chongqing University of arts and sciences, also in Materials Science and Engineering. Lei's thesis research is focused on studying the flexible solid-state supercapacitor. His research interests include nanomaterials for energy storage and conversion, triboelectric and hybrid nanogenerators, and novel materials processing techniques.

Zhongl-Li Liu obtained his Ph.D. in Atomic and Molecular Physics from the Sichuan University, Chengdu, in 2009. Now he is an associate professor in Luoyang Normal University. His research interests lie in theoretical and computational condensed matter physics including melting, solid–solid phase transitions under high pressure, and computational new materials design. He maintains two packages named MUSE and PHASEGO for the computational new materials design. His current interests are also in the computational design of gas-sensors via first-principles simulations.

Long Jin received his B.E. from Southwest Jiaotong University in 2015. He is currently pursuing a master's degree in materials science and engineering at Southwest Jiaotong University under the guidance of Professor Weiqing Yang.

Binbin Zhang was born in March 1994. He received his B.E. from Southwest Jiaotong University in 2015, and then became a graduate student in the school of materials science and engineering at Southwest Jiaotong University under the guidance of Professor Weiqing Yang.

Haitao Zhang received his M.S. in Materials Science and Engineering from Hainan University in 2011, and PhD in Institute of Electrical Engineering, Chinese Academy of Sciences in 2015. Currently, he is a lecturer at School of Materials Science and Engineering, Southwest Jiaotong University. His current research focuses on nano energy materials and electrochemical energy storage.

Minhao Zhu received his B.E. in metal materials science and engineering in 1990, M. S. in 1993, and PhD in 2001 from Southwest Jiaotong University. Now he is the professor of Southwest Jiaotong University, Yangtze River Scholar Distinguished Proffessor of China and National Outstanding Youth Fund Gainer. His current research focuses on Materials Science and Engineering, Mechanical Design and Theory.

Weiqing Yang received his M. S. in Physics in 2007, and PhD in Materials and Science Engineering in 2011. He was a post-doctorate research fellow at University of Electronic Science and Technology of China from 2011 to 2013. Subsequently, he was a post-doctorate research fellow at Georgia Institute of Technology from 2013 to 2014, under the supervision of Prof. Zhonglin Wang. Now he joined Southwest Jiaotong University as a professor. His current research focuses on nano energy materials, micro-nano devices, and optoelectronic devices.